Direct assessment of the shear behavior of strain-hardening cement-based composites under quasi-static and impact loading: Influence of shear span and notch depth / Tawfik, A.; Signorini, C.; Mechtcherine, V.. - In: CEMENT & CONCRETE COMPOSITES. - ISSN 0958-9465. - 140:(2023), pp. 105119-105119. [10.1016/j.cemconcomp.2023.105119]

Direct assessment of the shear behavior of strain-hardening cement-based composites under quasi-static and impact loading: Influence of shear span and notch depth

Ahmed Tawfik, Cesare Signorini, Viktor Mechtcherine

PII: S0958-9465(23)00193-2

DOI: https://doi.org/10.1016/j.cemconcomp.2023.105119

Reference: CECO 105119

To appear in: *Cement and Concrete Composites*

Received Date: 24 January 2023

Revised Date: 16 April 2023

Accepted Date: 3 May 2023

Please cite this article as: A. Tawfik, C. Signorini, V. Mechtcherine, Direct assessment of the shear behavior of strain-hardening cement-based composites under quasi-static and impact loading: Influence of shear span and notch depth, *Cement and Concrete Composites* (2023), doi: https://doi.org/10.1016/j.cemconcomp.2023.105119.

Direct assessment of the shear behavior of strain-hardening cement-based composites under quasi-static and impact loading: influence of shear span and notch depth

Ahmed Tawfik[1*], Cesare Signorini[1], and Viktor Mechtcherine[1]

[1] Institute of Construction Materials, Technische Universität Dresden, 01062 Dresden, Germany

* Corresponding author: ahmed.tawfik@tu-dresden.de

Abstract. Strain-hardening cement-based composites (SHCC) represent a new frontier for improving the resistance of concrete structures against highly dynamic loading regimes, *e.g.*, in the case of impact. A novel testing device was designed to characterize the shear behavior of such pseudo-ductile cementitious composites, whose dynamic response is extremely complex. The newly developed shear testing device was adapted to investigate the performance of fiber-reinforced, cementitious composites under both quasi-static and impact regimes. In the framework of setup validation and standardization, this article focuses on the investigation of the shear behavior of SHCC specimens and spotlights the influence of two main experimental shear parameters: shear span and notch depth. The purpose-specific shear device was integrated into a hydraulic testing machine and a gravity Split-Hopkinson tension bar (SHTB) for quasi-static and impact shear experiments, respectively. Shear spans of 2 mm and 5 mm were introduced by modifying the test setup. Furthermore, the specimens were shaped through sawn U-notches with varying depths of 3 mm, 5 mm, and 7 mm. The shear response of the SHCC specimens was monitored by means of Digital Image Correlation (DIC), which enabled the accurate derivation of strain fields, cracking behavior, and fracture modes on the specimen surface. The results showed that both shear span length and notch depth regulate the shear/tension fracture propagation. With an appropriate shear specimen shape, the desired dominant shear fracture could be obtained.

Keywords: SHCC, ECC, quasi-static shear, impact shear, cementitious composite, DIC.

1 Introduction

Strain-hardening cement-based composites (SHCC), also known as engineered cementitious composites (ECC), are cement-based, fiber-reinforced composite materials with superior tensile resistance and damage tolerance. Indeed, SHCC exhibit multiple cracking and strain hardening beyond first cracking stress, owing to the bridging action exerted by the embedded microfibers. Contrary to common fiber-reinforced concrete (FRC), which tends to exhibit strain-softening immediately after cracking, damage localization occurs in SHCC at a higher extent of strain, thus recalling the typical tensile trend of metals [1]. Such mechanical behavior leads to a variety of extremely beneficial characteristics, the most notable of which is a very high strain capacity accompanied by formation of very narrow cracks [2]. These peculiarities make SHCC an excellent choice for a wide range of applications where high ductility and durability are required, being applied as a complementary strengthening layer or as primary material for structural elements subject to sudden dynamic loading such as caused by impacts or blasts [3,4]. A key advantage of SHCC consists in the possibility of its tailoring to meet specific structural performance requirements by adjusting the mix design. Indeed, the micromechanical behavior of SHCC is governed by several measurable parameters related to the mechanical and chemical properties of the cementitious matrix, the fibers, and the fiber/matrix interface, leading eventually to effects on macroscopic behavior [5].

The behavior of SHCC under tensile and compressive loading has been extensively investigated and understood over the last decades [6–9]; however, their behavior under shear loading needs to be investigated further. Sound direct testing methods are highly appropriate to this aim. The structural performance investigation of SHCC beams tested in three-point bending experiments has been the subject of several publications [10–12], pointing out the enhanced shear capacity of the SHCC beams as compared to plain concrete (PC), reinforced concrete (RC), and fiber-reinforced concrete (FRC). According to Li *et al*. [13], shear responses of PC, FRC, and ECC mirror their respective tensile properties; it was shown that the shear structural performance of ECC beams was superior compared to the other composites. Moreover, shear properties of SHCC were indirectly described by Kanakubo *et al*. [14] through controlled axial tensile loading applied until a certain crack opening was reached. This facilitated the analysis of the shear transfer mechanisms depending on the crack opening. Direct shear characterization of SHCC beams was attempted by Van Zijl *et al*. [15] based on the Iosipescu shear setup. It was shown that the shear strength increased with increasing fiber volume and that specimens with fiber below 2% by volume were characterized by a mixed shear-flexure failure mode. The shear performance of three types of SHCC using four different combinations of torsional-axial stress was investigated in the recent paper by Figueiredo *et al*. [16]. The findings revealed once again a close relationship existing between shear performance and tensile behavior.

Against this background the need for robust and direct characterization protocols on the material scale of complex composites under high strain-rate shear loading is still compelling. Several shear testing setups already exist for testing composite materials under high loading rates. Among those, the punch-through shear (PTS) setup that was developed by Lukic and Forquin [17], for testing cylindrical concrete specimens in a split-Hopkinson pressure bar (SHPB). Adopting a similar specimen geometry, Cadoni *et al.* [18] developed a mechanical device to accommodate a shear specimen in a SHPB and allow shear dynamic testing of ultra-high performance fiber-reinforced concrete (UHPFRC). The double-shear specimen (DSS) geometry, initially designed for SHPB for characterizing the strain-rate-sensitivity of metals [19] [20] [21] [22], was used by Ngo and Kim in a strain-energy frame impact machine (SEFIM) to test UHPFRC.

In the current work, a mechanical shear device, recently developed by the authors [23], was employed to benchmark shear properties of SHCC. The mechanical device is based on the DSS geometry and was integrated in a gravitational Split-Hopkinson tension bar (SHTB), as well as a hydraulic testing machine to perform impact and quasi-static shear testing, respectively. Compared to the shear setups previously presented in the literature, the geometrical features of the shear device at hand warrant the accurate monitoring of cracks initiation and propagation throughout the whole duration of the test, through optical measurements. This is pivotal to an accurate derivation of the specimen response, in terms of deformations and mode of fracture. Furthermore, this specific shear testing device can be integrated into both tension and compression Split-Hopkinson bar setups, as well as into any hydraulic universal testing machine. This versatility entails reliable and reproducible evaluation protocols when assessing the specimen behavior at different loading rates, as specimen size, loading configuration, and boundary conditions are preserved.

Several parameters influence the shear behavior and failure mode of cementitious composites, including the geometrical features of the specimen, loading configuration, and boundary conditions. To achieve a reliable material characterization under shear loading, those testing parameters should be finely tuned and optimized. The most important parameter when defining the loading configuration of a shear experiment is the shear span length (a), defined as the distance between the loading point and support. Increasing the shear span length results in a flexural-shear mixed behavior, while decreasing it may lead to a more direct shear fracture [24]. Among the geometrical features of a shear sample, are the notches grooved into it. The presence of notches in shear samples is also crucial to funnel the shear crack propagation within a specified path. In this regard, the notch depth affects the shear/tension fracture propagation [18], as deeper notches increase the likelihood for a shear fracture to form prior to tensile failure [25]. Combining shear span length and notch depth allows the definition of a key parameter governing the shear strength and failure of cementitious composites under shear loads, namely the shear-span-to-effective-depth ratio (*a/d*) [24,26]. *d* is defined as the *shear ligament*, i.e. the height of the specimen net of the upper and lower notch depth in the region where shear failure is expected.

This paper originally presents a parametric investigation conducted on SHCC notched specimens to systematically assess the role of shear span length (*a*) and notch depth on the shear performance and failure mode of the specimens, evaluated through both quasi-static and impact direct shear experiments. The main target consists in optimizing the aforementioned parameters for this newly developed shear testing device in order to hamper undesired failure mechanisms such as crushing due to compression or failure due to dominant tension.

Thus, the novelty of this work consists not only in the tailoring of basic shear parameters for direct shear testing and adequate evaluation protocols, but also in the dynamic shear testing of SHCC, which represents a benchmark on its own. This study is intended as a basis for further optimization of the direct shear testing device, in terms of geometry and material, with the aim of establishing a sound protocol for characterizing various sorts of fiber-reinforced composites.

2 Materials and Methods

2.1 SHCC composition and specimen production

The investigated SHCC is composed of a cementitious matrix and ultra-high molecular weight polyethylene (UHMWPE, hereafter PE) fibers added in a volumetric fraction of 2%, and the detailed composition is presented in **Table 1**. This specific dosage was chosen on account of previous studies [2,5,6], which demonstrate that a strain capacity up to 3% is warranted, being particularly attractive in the practice as thin reinforcement layer for damaged concrete structures to improve their impact safety. Such tensile properties are reflected on the shear behavior of the composites, providing a better shear transmission across the crack resulting in a high ductility [13–15].

Preliminary compression experiments conducted on the cementitious matrix yielded a mean compressive strength of around 60 MPa. The PE fibers are produced by DSM, the Netherlands, under the brand name Dyneema SK60 [27]. The fibers are 6 mm-long with an average diameter of 18 µm, a tensile strength of 2500 MPa, and Young’s modulus of 80 GPa. They are characterized by pronounced hydrophobicity, which induces a relatively weak frictional bond with the cementitious matrix.

Table 1

Composition of the SHCC under investigation.

Components	**Dosage** [kg/m³]
Cement CEM I 52.5 R-SR3/NA	506
Fly ash	620
Quartz sand (0.06-0.2 mm)	536
Viscosity modifying agent	2
Superplasticizer Glenium ACE 460	11
Tap water	350
PE fibers (2% by volume)	20

A 3-liter batch of SHCC mixture was mixed in a 5-liter volume Hobart mixer. The overall water-to-binder ratio was 0.3. The fresh mixture was cast in steel prismatic molds of dimensions 160 mm × 40 mm × 40 mm. From each prism, two shear specimens, each with dimensions of 70 mm × 40 mm × 21 mm were obtained, see **Fig. 1a**. The U-shaped notches were then sawn into the specimen by means of a 1-mm cutting blade, as presented in **Fig. 1b**. The notch depths of 3 mm, 5 mm and 7 mm were chosen to result in shear ligaments of 15 mm, 11 mm, and 7 mm, respectively, with respect to the specimen depth. Eventually, a high-contrast speckled pattern for optical measurements was applied onto the lateral face monitored by a stereo camera system.

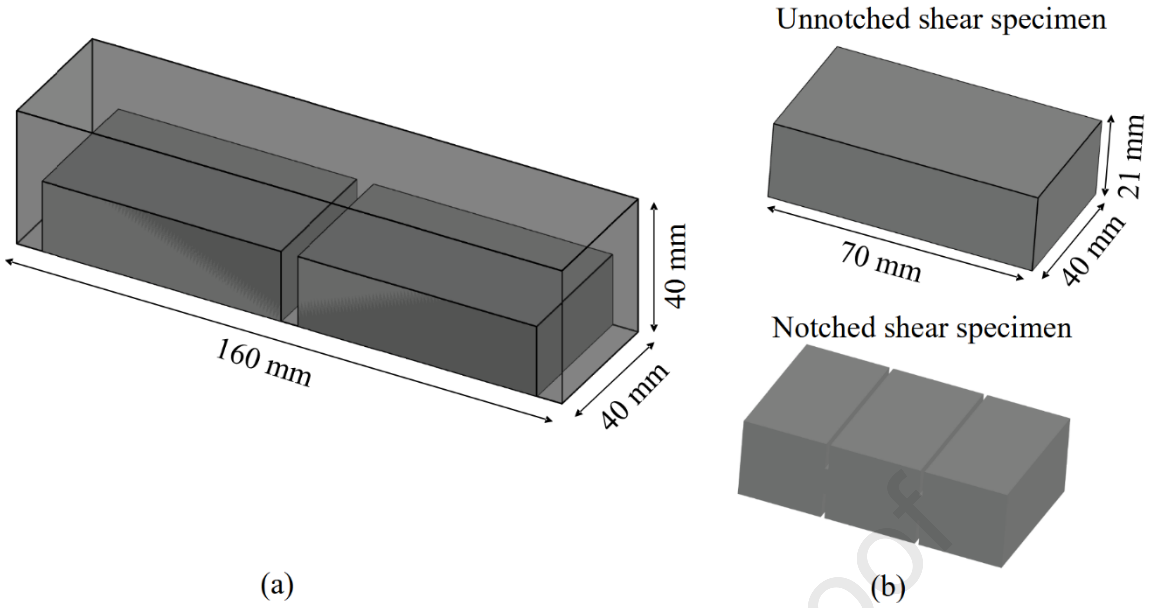

(a) (b)

Fig. 1. (a) Prismatic mold for casting (compliant with UNI EN 196-1) and (b) shear specimen cut from the mold, before and after notching.

2.2 Test setups

2.2.1 Quasi-static shear test setup

The quasi-static shear test setup consisted of a hydraulic universal testing machine (UTM) (Instron 8501, USA) equipped with a novel mechanical shear device and a stereo optical camera system (Aramis adjustable 12M by GOM, Germany), as shown in **Fig. 2a**. The mechanical shear device was specifically designed to characterize pseudo-ductile cementitious composites, and its configuration is based on the well-known double-shear-specimen experiments (DSS) [19,20]. The development of the mechanical shear device and its application with the SHTB was presented in the recent publications by Tawfik *et al*. [23,28]. It consists of three metal pieces: the upper and lower adapters and the loading plate; see **Fig. 2b**. The loading plate is connected to the lower adapter through high-strength steel bolts, forming a single rigid part, Part 1. This rigid part is responsible for applying the load to the shear sample through the loading plate, as indicated in **Fig. 2b** by the red arrows. The upper adapter defines Part 2 of the shear device, which serves as the support and generates the reaction force equal to the force applied by Part 1, as indicated by the green arrows in **Fig. 2b**. The shear span length defines the horizontal distance between the loading point and the support (Part 1 and Part 2); see **Fig. 2c**. The shear device was incorporated in the Instron machine using two short cylindrical brass bars to connect the adapters to the crossheads of the UTM. The stereo optical system was used to monitor the movement of the two parts of the shear device along with the shear zones indicated in **Fig. 2c**, with a frame rate of 4 Hz. The acquired frames were processed using the digital image correlation (DIC) software GOM Correlate Professional (Carl Zeiss GOM Metrology GmbH, Germany). From this DIC analysis full field of displacements and strains on the specimen surface (shear zones) were obtained, and crack propagation and failure modes occurring during the test were tracked and assessed. To this aim, a black and white stochastic pattern was painted on the shear zones of the specimen facing the optical sensors; see **Fig. 2c**. Specimens were loaded at a controlled displacement rate of 0.05 mm/s. The lower crosshead is movable and connected to the lower shear adapter, whereas the upper crosshead is fixed and connected to the upper adapter. With this configuration, the shear forces are applied within the shear span. To prevent lateral deformation and rotation of the specimen, as indicated by lateral arrows in **Fig. 2b**, a bi-component epoxy adhesive was adopted to glue the specimen to the shear device at all the contact points. The epoxy adhesive has an inherent strength of 12 MPa, which warranted a good shear fracture of the specimen by providing sufficient confinement and prevention of lateral dilation of the shear specimen. During quasi-static experiments, the force acting on the specimen was directly measured by the UTM load cell.

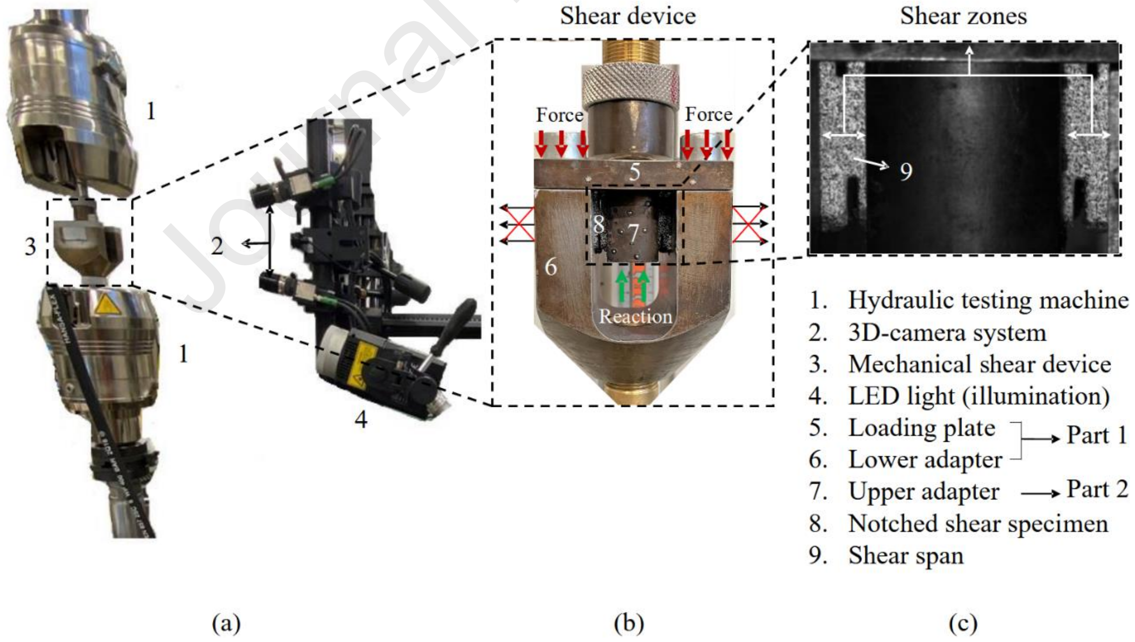

(a) (b) (c)

Fig. 2. (a) Quasi-static shear test setup, (b) mechanical shear device, and (c) shear spans (shear zones) recorded by the optical sensors for DIC analysis.

2.2.2 Impact shear test setup

The aforementioned versatile shear device was also integrated into a recently developed gravity-driven Split-Hopkinson Tension Bar (SHTB) [8], to perform impact shear experiments. The setup is shown schematically in **Fig. 3a**, where the shear device is threaded between the input and transmitter bars, *i.e.*, lower adapter threaded to input bar and upper adapter threaded to the transmitter bar. The elastic bars are made of brass with a 24 mm diameter each, at which the input bar has a length of 1310 mm, while the transmitter bar has a length of 2500 mm. The loading configuration and boundary conditions are similar to the quasi-static case.

The input wave is generated by dropping the 30 kg steel impactors from any height up to 3.7 m on the steel flange. Following fundamental energy principles, the strain rate can be adjusted by varying the initial position of the impactors, the generated input wave being based on the rigid body motion of the steel impact flange [29]. Once the wave is generated, it propagates through the input bar, then through the shear device, which loads the specimen in shear, and eventually through the transmitter bar.

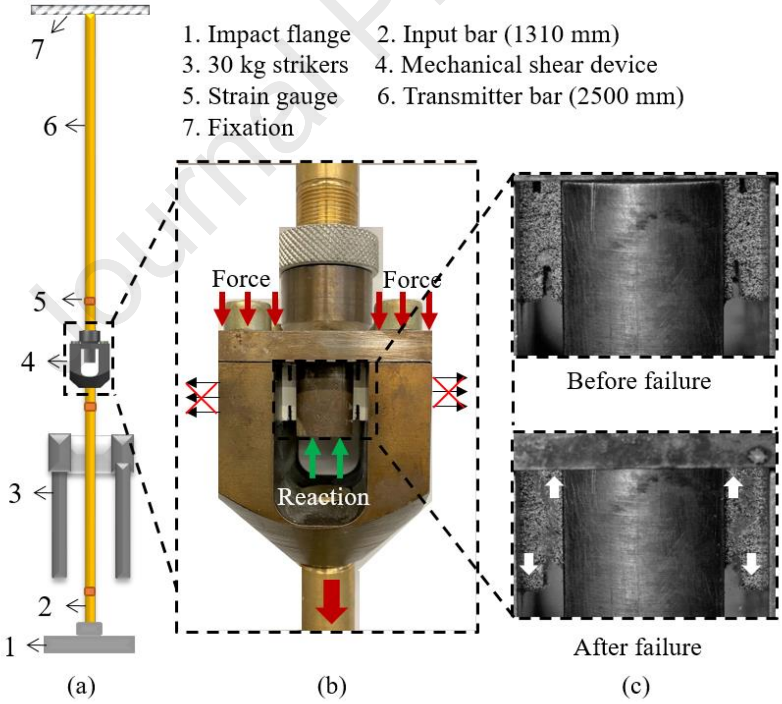

Fig. 3. (a) Gravitational Split-Hopkinson tension bar (SHTB) with the integrated mechanical shear device, (b) mechanical shear device elaborating the loading configuration, and (c) frames recorded by the high-speed cameras during the experiment.

The optically recorded frames before and after failure are shown in **Fig. 3c**. For the impact shear experiments conducted in this work, the drop height of the impactor was set at 0.65 m, which resulted in an impact velocity of 3.5 m/s and shear strain rate up to 2000 s^{-1}. Strain gauges were glued to both bars to record the input, reflected, and transmitted waves. Data from the strain gauges were acquired using a high-speed data acquisition system (DEWEsoft, Slovenia), with a recording frequency of 1 MHz. For the optical measurements, high-speed cameras (SA-X2, 480K-M1, Photron, Japan) were employed. The frame rate of the cameras in the impact shear experiments was 112500 Hz. In similar fashion to quasi-static experiments, the specimen was also glued to the shear device during the impact experiments to provide sufficient confinement and avoid a dominant tensile fracture mode, as noted by the authors in previous publications [23]. In general, for tensile and compressive Split-Hopkinson bar experiments, stress equilibrium is attained before failure of the specimen, and the apparent response of the specimen is based on the average force obtained on the input bar (input + reflected force) and transmitter bar (transmitted force) [6,30]. This allows derivation of the specimens' responses and deformations using the one-dimensional wave propagation theory [31]. In the current impact shear experiments, stress equilibrium was not attained in the specimen before cracking due to the influence of the mass and geometry of the shear device on wave propagation. This was concluded by comparing the input plus reflected wave to the transmitted wave recorded on the elastic bars and was explained in detail by the authors in a previous study [23]. Therefore, for impact shear experiments conducted in this work, the force in the shear specimen was based only on the transmitted wave recorded on the transmitter bar. Again, deformations and fracture modes of the shear specimen were measured based on the optical recordings of each experiment, as obtained by the 3D-camera. The recorded frames were then analyzed by the DIC technique [28].

2.3 Experimental program

Before presenting the experimental program conducted in the present work, a research road map is presented in **Fig. 4**, to frame its significance within the overall research workflow. First, a novel mechanical shear device that could be integrated in the SHTB was developed, as already presented in **Fig. 3**b. Design was conducted using numerical approaches, capable of estimating wave propagation and quantifying possible artifacts due to the mass and geometry of the device. Second, the developed shear device was validated by testing pseudo-ductile composites, i.e., SHCC, and performing detailed crack analysis to assess and appraise the failure mode of the specimens [23,28]. Eventually, in this work the main shear parameters influencing the shear behavior and fracture mode of the specimens (i.e., shear span length and notches depth) are studied and optimized, with the purpose of establishing a sound testing protocol for dynamic characterization of cementitious composites under dominant shear conditions. Further aims include optimizing the shear device based on the optimized parameters from this work as well as wave artifacts from previous works. Investigations aimed at reducing and quantifying structural inertia effects are object of ongoing research.

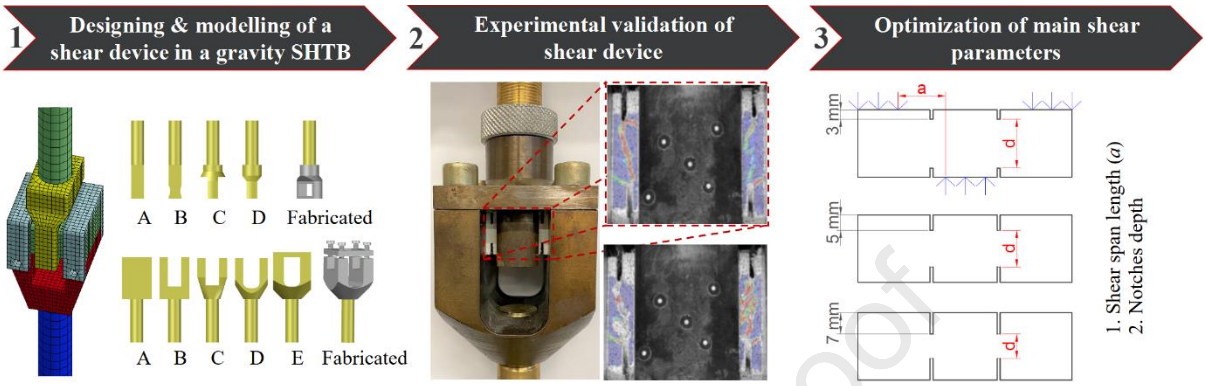

Fig. 4. General research road map presenting the aims of the authors in previous, current, and future research. The current work is represented in the third inlet.

To achieve the target envisaged in **Fig. 4** (inlet 3), quasi-static and impact shear experiments were carried out by varying the two parameters under investigation: shear span length and notches depth. A road map describing the experimental workflow is presented in **Fig. 5**. Initially, the optimal shear span length was ascertained through quasi-static test series only, while the notches depth was kept constant. Afterwards, the notches depth was varied keeping the optimal shear span length constant, in both static and impact regimes.

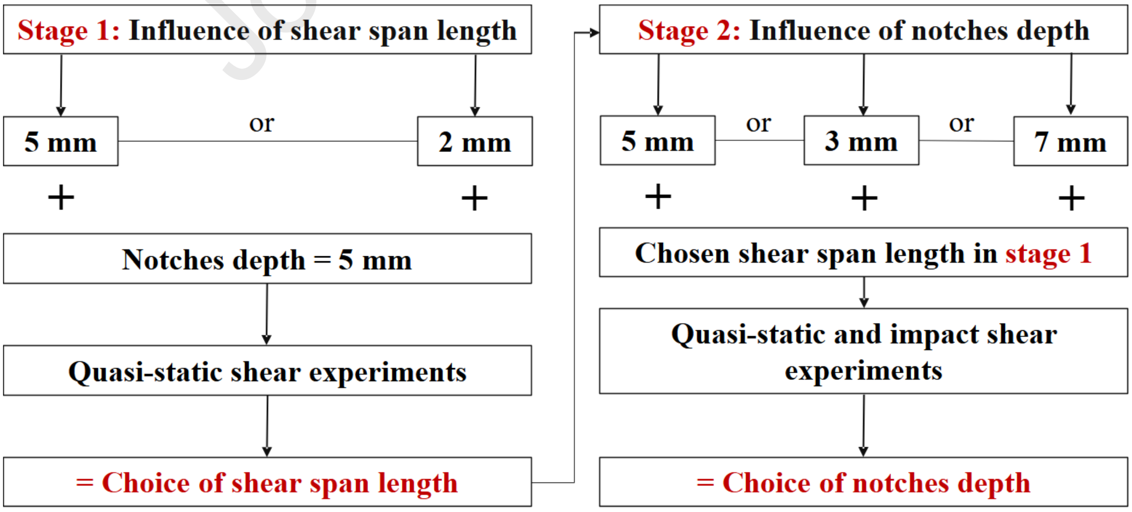

Fig. 5. Road map describing the experimental workflow followed in this work.

Table 2 summarizes the experimental program performed in this work, where each experiment is denoted with respect to its testing parameters and configuration. First, to investigate the influence of the shear span length, samples with 5 mm and 2 mm shear span lengths were tested only under a quasi-static loading regime, where the notch depth was kept constant at a value of 5 mm, resulting in a/d values of 0.45 and 0.18, respectively. The depth (d) was computed by subtracting the depth of both top and bottom notches from the specimen whole depth. With a displacement rate of 0.05 mm/s applied in the quasi-static regime, shear strain rates of 0.01 s^{-1} and 0.025 s^{-1} were attained for the 5 mm and 2 mm shear span lengths, respectively. Such a difference in these low ranges of shear strain rate should not influence the comparability between the two shear span lengths and structural effects such as inertia should be negligible [32,33]. Second, the influence of the notches depth was studied by means of samples sets possessing three different notch depths, *i.e.*, 5 mm, 3 mm, and 7 mm, where the shear span length was kept constant with the value of 2 mm. Both quasi-static and impact loading regimes were investigated, at which shear strain rates up to 0.025 s^{-1} and 2000 s^{-1} were attained, respectively. The reason for selecting the 2-mm shear span length is traced back to the evidence obtained from experiments conducted in the quasi-static regime and is discussed in the Results Section. The three notch depths, 5 mm, 3 mm, and 7 mm, resulted in a/d ratios of 0.18, 0.13, and 0.28, respectively, see **Table 2**.

Table 2
Summary of the experimental program. Experimental series 1-2 aimed at determining the optimal shear span (SS) length, while experimental series 2-7 aimed at determining the optimal notches depth (ND).

#	Experiment label
1	SS 5mm – ND 5mm – a/d 0.45 – Quasi-static (QS)
2	SS 2mm – ND 5mm – a/d 0.18 – Quasi-static (QS)
3	SS 2mm – ND 5mm – a/d 0.18 – Impact (IM)
4	SS 2mm – ND 3mm – a/d 0.13 – Quasi-static (QS)
5	SS 2mm – ND 3mm – a/d 0.13 – Impact (IM)
6	SS 2mm – ND 7mm – a/d 0.28 – Quasi-static (QS)
7	SS 2mm – ND 7mm – a/d 0.28 – Impact (IM)

The specimens are labelled as follows: The first part defines the shear span length (SS), the second part defines the notch depth (ND), the third part defines the a/d ratio and the fourth part defines the loading rate. For example, 'SS 5mm – ND 5mm – a/d 45 – Quasi-static (QS)' denotes a sample with a shear span length of 5 mm, notch depth of 5 mm and a/d of 0.45, tested in quasi-static regime. In total, seven different configurations were tested in this study, considering three repetitions within each series. For quick identification, the seven different experimental configurations are numbered from 1 to 7, as shown in **Table 2**.

2.4 Testing configurations

As mentioned in Section 2.1, applying different notch depths to the shear sample was done in a straightforward way by using a saw blade. The challenging task was to vary the shear span length in the shear device. To tune the shear span length, two different loading plates were produced. Since the loading plate serves as the loading part, changing its dimensions and geometry results in changing the position of the loading points, and hence, the shear span (zone) dimensions could be controlled. The two different shear samples configurations with respect to the shear span length are presented in **Fig. 6a**. The shear force diagram for each shear span length case is presented, indicating locations of the maximum shear forces zones. Decreasing the shear span length results in a narrower shear zone limiting the shear crack propagation to a smaller region with concentrated shear force.

For the 5 mm shear span length sample, the horizontal distances between both loading plate and lower adapter, which are screwed together, and upper adapter are the same, equaling 5 mm. The top and bottom notches are applied in the middle of the shear span; see **Fig. 6b**. With a 1 mm notch width, the distance between the edges of the notches and the adapters is 2 mm. For obtaining a 2 mm shear span length, the inner dimensions of the loading plate were increased by 3 mm, decreasing the horizontal distance between the loading plate and the upper adapter to 2 mm which corresponds to the shear span length; see **Fig. 6c**. The notches were applied in the middle of the 2 mm shear span length, leaving a horizontal distance of 0.5 mm between the notches edges and both the loading plate and upper adapter. While the distance from the notches edges to the lower adapter was 3.5 mm. Since the force is produced solely by the loading plate, the lower adapter was not changed in both shear span cases.

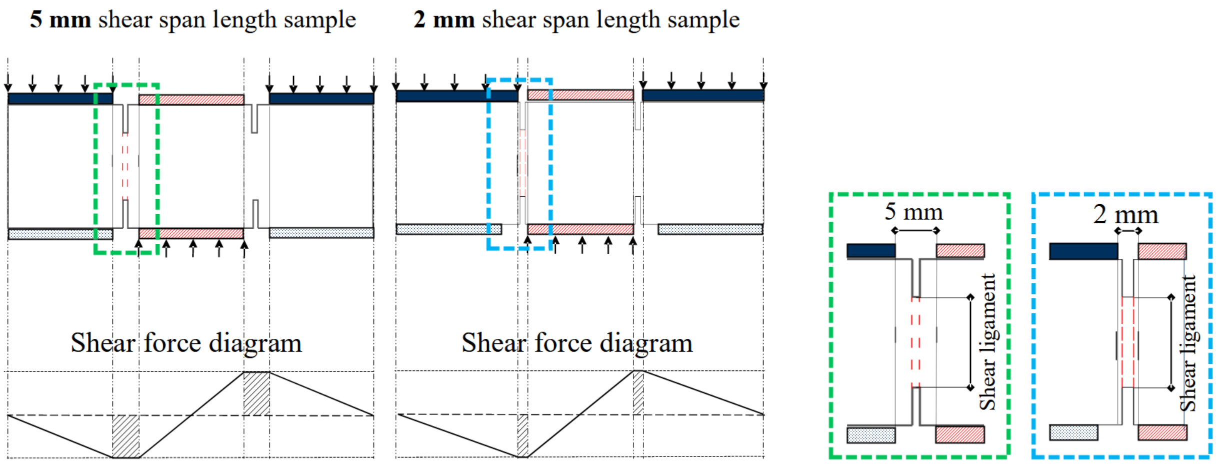

(a) (b) (c)

Fig. 6. (a) 5-mm and 2-mm shear span lengths within the sample; the dotted hatch indicates the lower adapter, and solid hatch indicates the loading plate (loading part), along with shear force diagrams for each case indicating the maximum shear force regions (black hatched areas); red hatch indicates the upper adapter (areas where reaction forces are exerted). Zoomed view of the 5-mm (b) and 2-mm (c) shear spans, with respect to the shear adapter parts.

3 Results and discussion

3.1 Quasi-static shear experiments

According to **Table 2**, experiment series 1 and 2, aimed at investigating the behavior of SHCC samples with different shear span lengths under quasi-static loading conditions. The corresponding experimental results are presented in **Fig. 7** and **Fig. 8** in the form of force vs vertical displacement diagrams synchronized at different stages with images acquired by the optical sensors and processed with DIC showing the full field measurement of the “major strains” in the two shear zones. Major strain is the largest possible principle strain resulting from the principle axis transformation of the strain tensor and was calculated, in the DIC software, according to the equation stated in [34]. This enabled the measuring and tracking of cracks initiation and propagation throughout the experiment. For the typical sample with 5-mm shear span length (SS 5mm – ND 5mm – a/d 0.45 – QS), shown in **Fig. 7**, tensile cracks formed once the sample was loaded, at locations where maximum principal tensile stresses are expected, *i.e.*, at the inner edges of the top notches and outer edges of the bottom notches. Such tensile cracks formed as the sample tried to accommodate bending, while this mechanism was restrained by the gripping conditions deliberately imposed by the shear adapters and by the glued portions, completely preventing the specimen from moving laterally or bending. The tensile cracks started forming at a force level of 3.9 kN up until almost 15 kN (Stages 1-3).

Afterwards, several inclined cracks started to form at the two shear zones between the top and bottom notches (Stages 4-5). At last, at a force level of 24.8 kN (Stage 6), the inclined cracks connected vertically together forming a major shear crack at one shear zone, followed by another major shear crack in the other shear zone (Stage 7). Both shear cracks slid continuously until complete failure of the specimen was achieved (Stage 8).

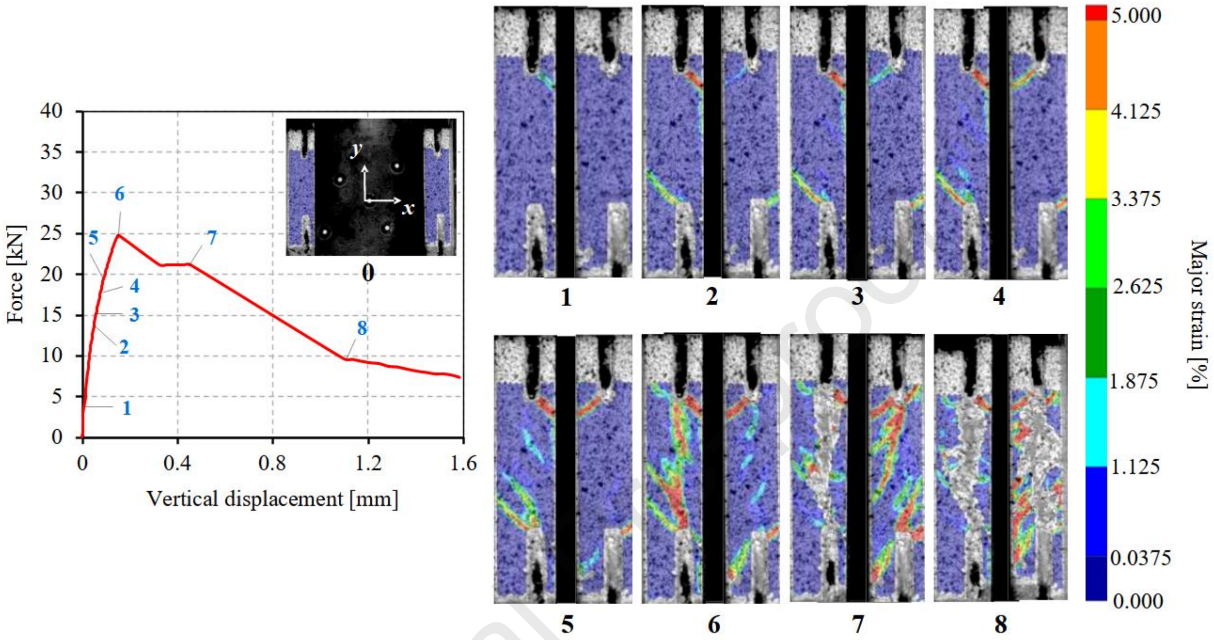

Fig. 7. Force vs vertical displacement of SHCC sample SS 5mm – ND 5mm – a/d 0.45 – QS (experiment series 1), synchronized with DIC frames illustrating a full field measurement of the major strains within the two shear zones.

Decreasing the shear span from 5 mm to 2 mm, as presented in **Fig. 8**, resulted in slightly different failure behavior. Indeed, in the latter configuration, the formation of any tensile cracks due to bending initiation at the inner edges of the top notches was hampered. This was due to the smaller horizontal distance, 0.5 mm, between the edges of the top notches to the loading plate, unlike the bottom notches, which had a much larger horizontal distance, 3.5 mm, to the lower adapter, as previously presented in **Fig. 6c**. Therefore, tensile cracks formed at the outer edge of the bottom notches, similar to observations in the 5-mm shear span length case since the specimen was still supported at the same position by the lower adapter, even counting on a larger horizontal distance between the lower adapter and the bottom notches. The bottom tensile cracks formed at a force level of around 5 kN and continued to form until a force level of 15 kN (Stages 1-2) was reached. This was along similar lines of counterpart accounting for the larger shear span in experiment series 1. Through stages 3-5, inclined cracks at both shear zones developed until two major cracks formed at a maximum force of around 28 kN, causing failure of the sample, as was observed for the larger shear span configuration. Finally, sliding of the two shear cracks continued until complete separation of the sample occurred (Stage 6).

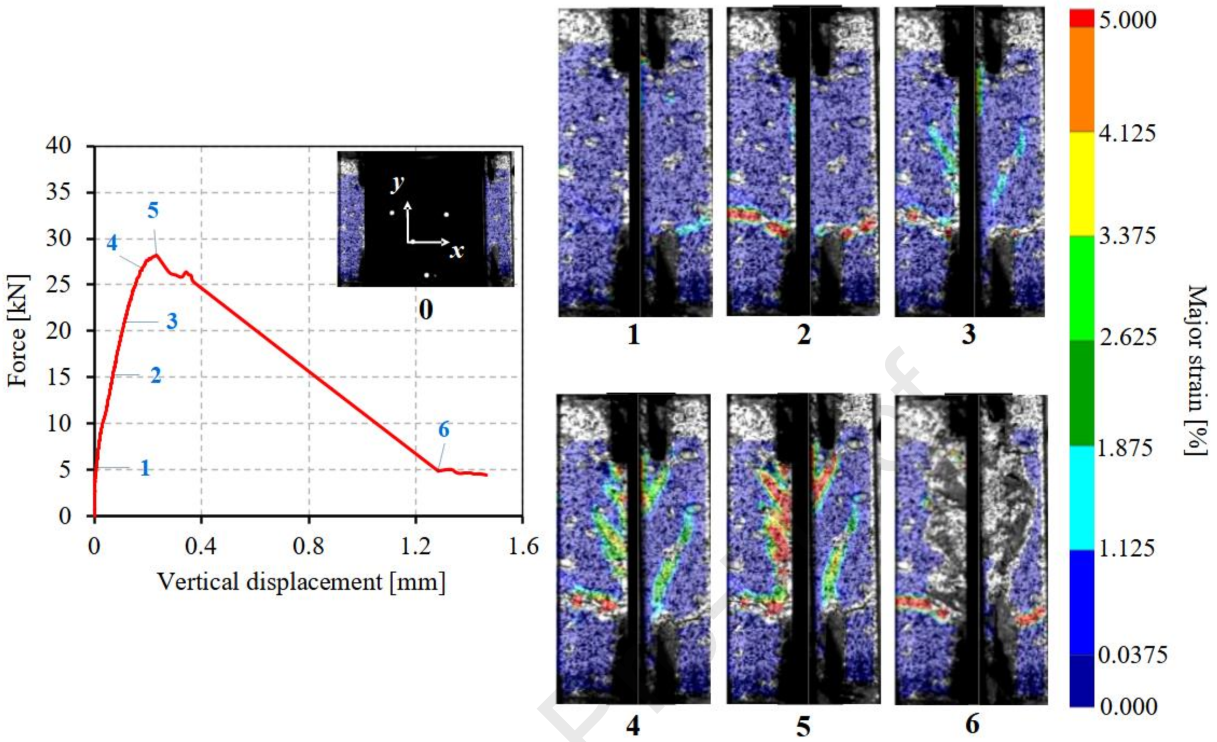

Fig. 8. Force vs vertical displacement of SHCC sample SS 2mm – ND 5mm – a/d 0.18 – QS (experiment series 2), synchronized with DIC frames illustrating a full field measurement of the major strains within the two shear zones.

Based on the experimental results presented in **Fig. 7** and **Fig. 8**, the 2-mm shear span length was considered for all forthcoming experiments conducted in this work, *i.e.*, experiment series 3-7. In fact, although failure and fracture mode did not differ distinctively among those observed in experiment series 1 and 2, closer distances between the support and the loading action were more likely pivotal for a neater shear fracture mode (mode II). This argument is consensually supported in the literature. Magnusson *et al*. [24] observed a sliding type shear failure occurring along a well-defined shear plane when a/d is less than 0.5. Similar conclusions were obtained by Bažant and coworkers in [35,36], stating that a vertical running shear crack occurred for a narrower shear zone, where the crack was inhibited in propagating sideways. Furthermore, by comparing the experiments in series 1 and 2, unsought tensile cracks at principle tensile stresses zones were hindered by reducing the extension of the pertaining zones, namely the distance between the load and support.

The second part of the quasi-static shear experiments, series 2, 4, and 6, aimed at understanding the influence of notch depth on the shear failure behavior of SHCC samples. Hence, while the shear span length was kept constant at 2 mm, the notch depths were varied from the initial value of 5 mm, investigated in experiment series 2 and shown in **Fig. 8**. More specifically, 3 mm, and 7 mm were selected, and the results under quasi-static shear loading are presented in **Fig. 9** and **Fig. 10**, respectively. As far as failure modes were considered, decreasing the notch depth from 5 mm to 3 mm, a sharp behavioral divergence was noticed. In the latter case, a shear-compression failure prevailed, and the sample failed due to the crushing of compressive struts that developed in the shear zones between the loading points and the support, as can be seen in **Fig. 9**. The fracture process started by the formation of a large diagonal crack at a force level of 20 kN (Stage 1). Then more diagonal cracks formed at both shear zones (Stages 2 and 3), until the maximum force of 39 kN was reached and failure initiated (Stage 4). In this case the failure occurred by crushing of the compressive struts formed between the diagonal cracks within each shear zone. Eventually, post-peak behavior is shown between stages 4 and 5, at which the sample is splitting near the two shear zones.

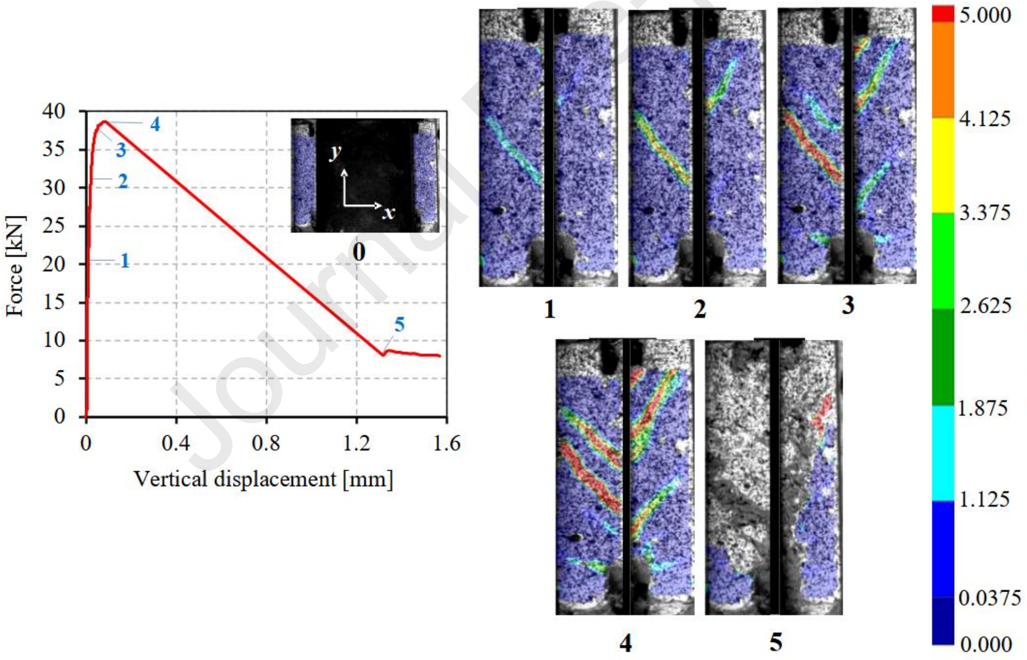

Fig. 9. Force vs vertical displacement of SHCC sample SS 2mm – ND 3mm – a/d 0.13 – QS (experiment series 4), synchronized with DIC frames illustrating a full field measurement of the major strains within the two shear zones

Conversely, increasing the notch depth from 5 mm to 7 mm resulted in the most favorable direct shear fracture, characterized by a sliding type of failure along the two well-defined shear planes. The failure process of a shear sample with 7-mm deep notches is presented in **Fig. 10**. As expected, at Stage 1 one tension crack formed at the bottom of each shear zone at a force level of about 6 kN and propagated during Stage 2. Then, at a force level of 23 kN, just before the maximum load was reached, one vertical shear crack started to form at each shear zone between the top and bottom notches (Stage 3). When the maximum load was reached at around 25 kN, the sample started failing by mutual sliding of the shear crack surfaces (Stage 4-5). Eventually, at stage 6, the sample is almost completely split.

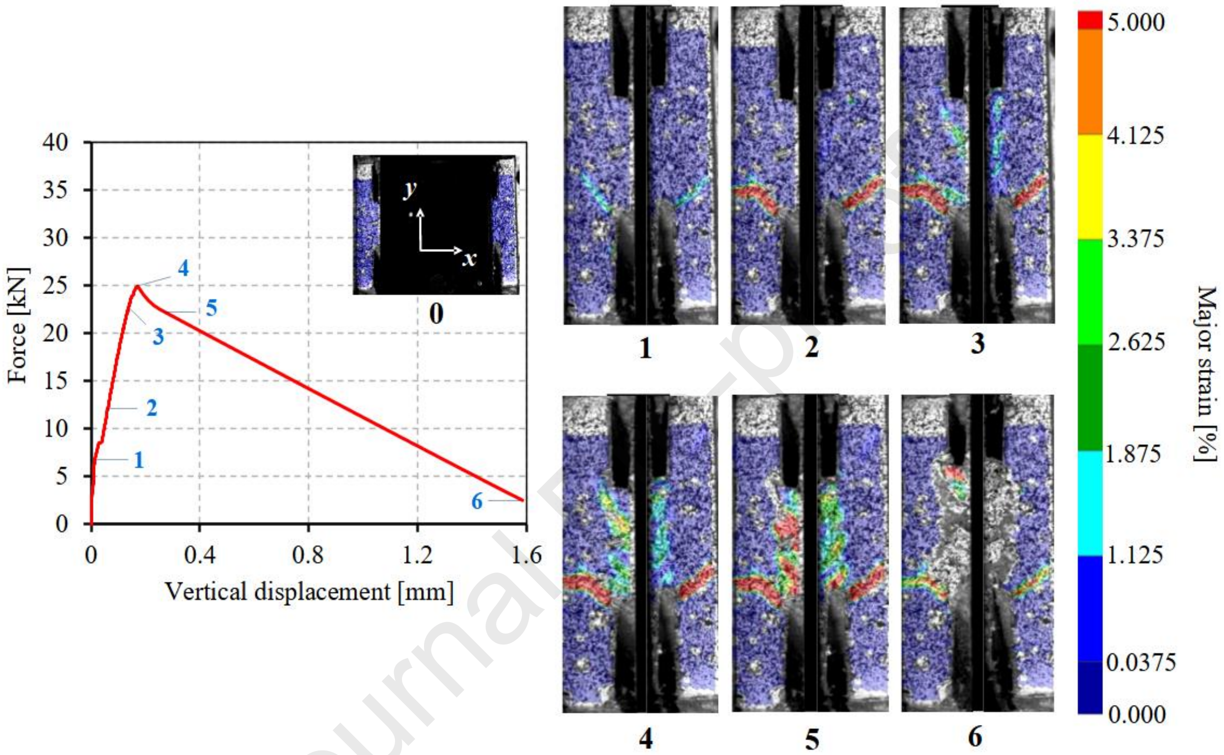

Fig. 10. Force vs vertical displacement of SHCC sample SS 2mm – ND 7mm – a/d 0.28 – QS (experiment series 6), synchronized with DIC frames illustrating a full field measurement of the major strains within the two shear zones.

3.2 Impact shear tests

The impact shear experimental results are presented in force vs vertical displacement curves and DIC sequential frames. As previously stated, the 2-mm shear span was chosen based on quasi-static experiments to attain dominant shear fracture. Experiments on SHCC shear samples with three different notch depths, namely 5 mm, 3 mm, and 7 mm tested in the impact regime are represented by experiment series 3, 5, and 7, respectively, as displayed in **Table 2**. Remarkably, shear samples with notches depths of 5 mm and 3 mm did not fail when tested under the impact regime, unlike samples with notches 7 mm deep; these samples fractured successfully under the applied input wave. This is revealed in **Fig. 11**, which shows, on the same frame, the applied and the transmitted force for the three notch-depth cases. It is worth remarking that the input wave generating the load was initiated by a weight falling from a height of 0.65 m, as explained in Section 2.2.2, and it is measured by the strain gauges at the lower end of the input bar for 650 μs before the arrival of the reflected wave from the sample. Therefore, the first input wave passage is valid for 650 μs, and this is indicated by the green-dashed lines in **Fig. 11**. The response of the sample with respect to the applied loading wave is represented by the transmitted force. It can be seen that for the smallest depth values of the notches, *i.e.*, 3 mm and 5 mm, the input loading wave was very long compared to the specimen with 7 mm-deep notches. The remaining part of the loading wave in excess of the 650 μs threshold is ascribed to further reflections and following input wave passages. As a result, the amplitude of the input force wave was insufficient to fracture the 3 mm- and 5 mm-deep notched samples, even after several wave passages. This can be seen in **Fig. 11a** and **Fig. 11b**, where the transmitted force did not evidence any descending or softening branch until the end of the experiment. On the contrary, the 7-mm-deep notched samples all failed from the first input wave passage, and the transmitted force reported in **Fig. 11c** mirrors the actual sample's response.

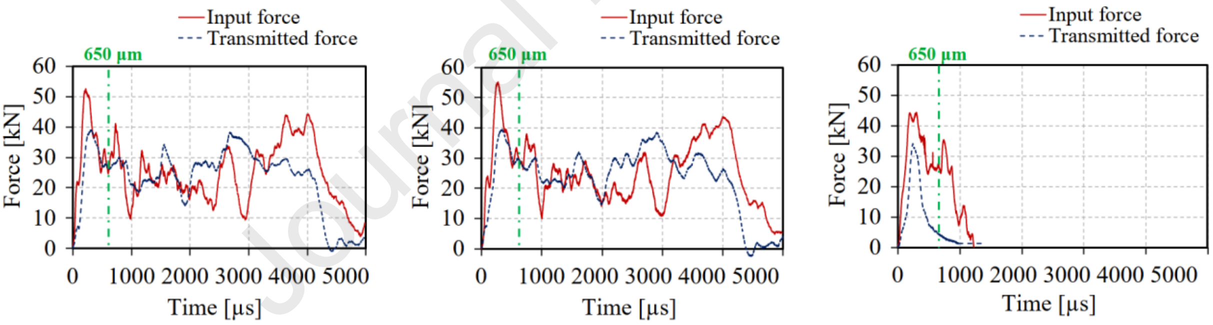

(a) (b) (c)

Fig. 11. Input and transmitted forces measured in impact shear experiments for (a) 3mm-, (b) 5 mm-, and (c) 7 mm-deep notched specimens, *i.e.*, the green-dashed lines indicate the time of the first input wave passage. Experiment series 5, 3, and 7, respectively.

In a manner similar to that of the quasi-static regime, the combination of the 7-mm deep notches and a 2 mm shear span length, *i.e.*, experiment series 6 and 7, resulted as well in a net shear sliding failure in the impact regime. This was due to the effective design of a clear shear zone, featuring a limited distance between the support and the loading point in combination with the notches, which were deep enough to allow the shear cracks to develop free of the influence of the self-confinement of the sample and, in addition, preventing a crushing failure. Furthermore, unlike in the quasi-static regime of experiment series 6, tensile cracks at the lower notches did not form, as shown in **Fig. 12**, where the fracture behavior of the 7-mm deep notched shear sample is presented during impact. The shear cracks started to form vertically during stages 2-4 and the fracture initiated when the tested sample reached its maximum apparent strength at stage 5 when two major shear cracks formed between the top and bottom notches. The shear cracks were almost vertical and resulted in crack sliding (Mode II), thus proving the dominant direct shear fracture mode. As already stated, no tensile cracks formed, contrary to what had been previously noticed by the authors [23,28] in considering samples having 5-mm shear span. In that configuration, tensile cracks always formed in correspondence with both the top and bottom notches.

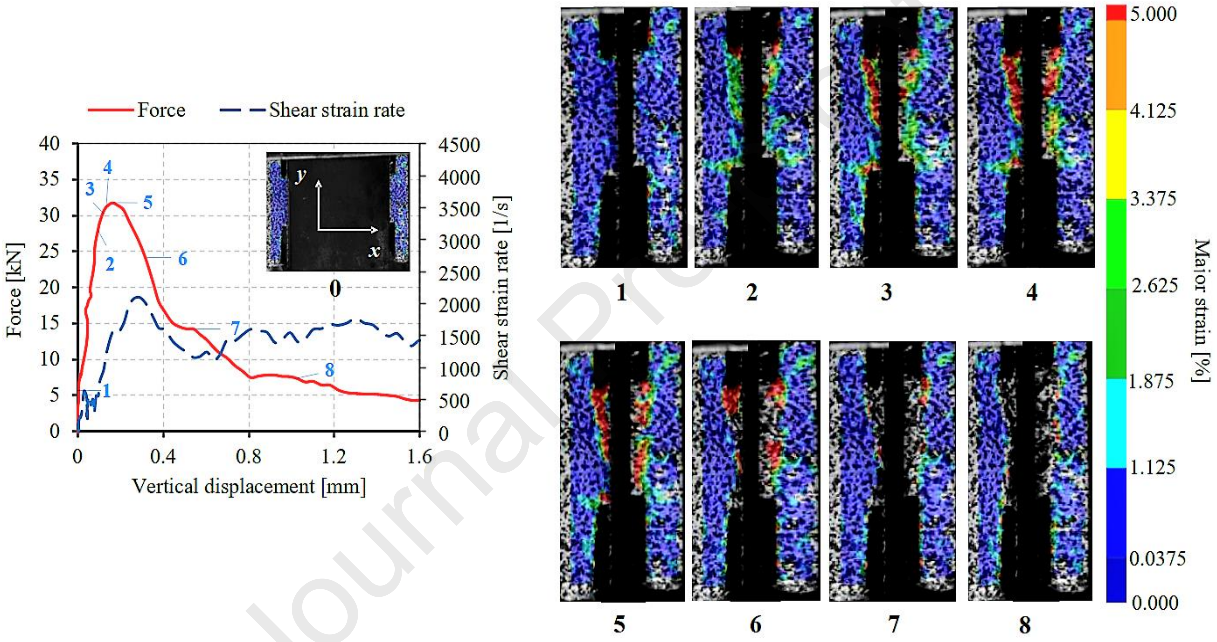

Fig. 12. Force and shear strain rate vs vertical displacement of SHCC sample SS 2mm – ND 7mm – a/d 0.28 – IM (experiment series 7), synchronized with DIC frames illustrating a full field measurement of the major strains within the two shear zones.

3.3 Discussion

3.3.1 Influence of the shear span length on failure mode in quasi-static shear experiments

The quasi-static experimental results of experiment series 1 and 2 enabled the establishment of the influence of shear span length on the response and failure behavior of samples subjected to shear loading. **Fig. 13a** and **Fig. 13b** compare the force vs vertical displacement curves for samples with 5-mm and 2-mm shear span lengths, respectively, and with notches depths of 5 mm. A higher peak force was consistently attained for the 2-mm shear span samples. This is made explicitly clear in **Fig. 13c**, where the maximum forces obtained for fracturing the shear samples are presented. The distinct divergence found in the shear strength values can be explained by assessing the fracture behavior in depth. First, in the 5-mm shear span case tensile cracks at both the top and bottom notches formed. Such cracks are a result of principle tensile strains forming perpendicular to the principle tensile stresses at the notches edges and form as the sample tries to bend. Where for the 2-mm shear span length case tensile cracks at the top notches were hindered, this resulted in a high shear force required for failure. Furthermore, failure in the case of 5-mm shear span case was associated with the formation of several inclined tension cracks extending at the relatively larger shear zone, interconnecting later to form two major shear cracks. For the 2-mm shear span length samples, a net vertical fracture was triggered at each shear zone, which was much less affected by capillary tensile cracks.

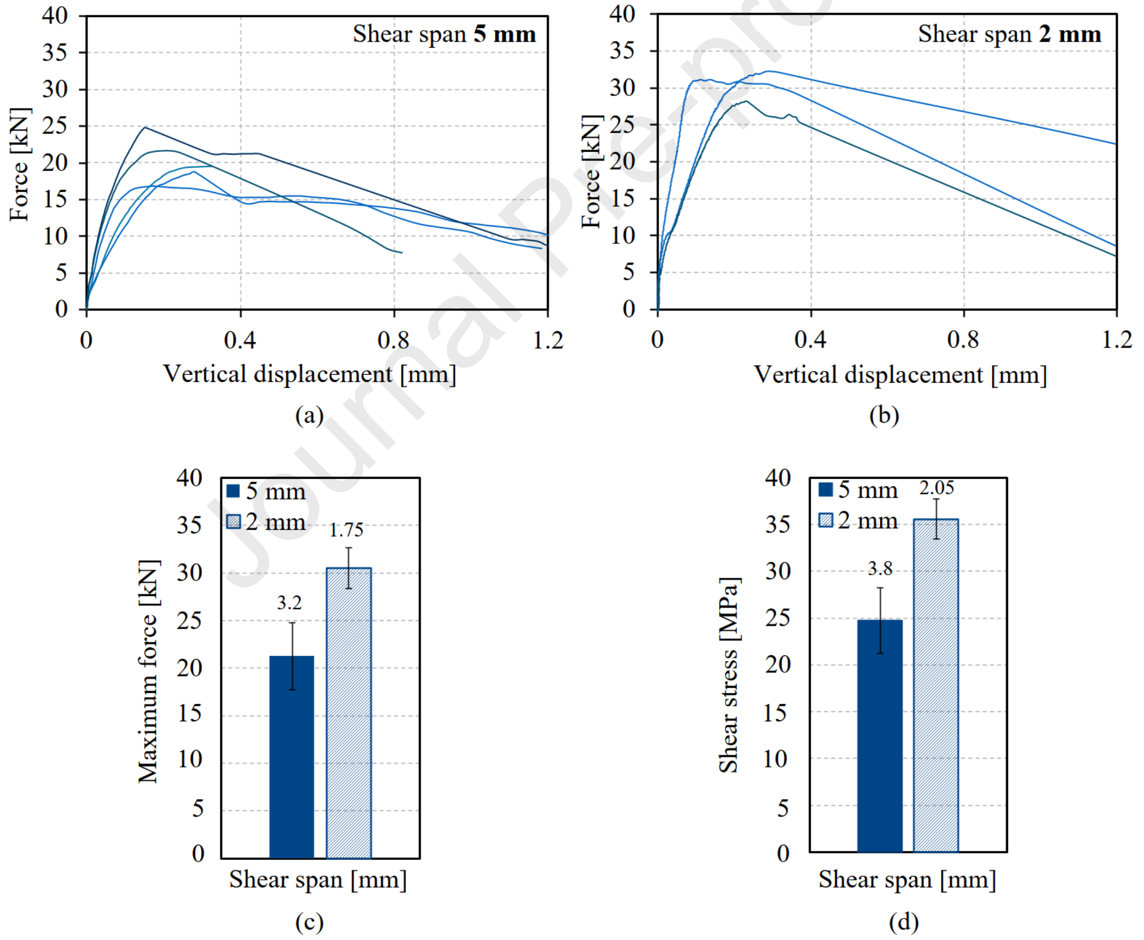

(a) (b)

(c) (d)

Fig. 13. Quasi-static test results of shear samples with 5 mm deep notches and with 5 mm or 2 mm shear span length, experiment series 1 and 2, respectively. (a) Force vs vertical displacement for (a) 5 mm shear span length and (b) 2 mm shear span length, (c) maximum forces, and (d) shear stresses. Numbers above the bars represent standard deviations.

From a geometrical standpoint, the higher bearing capacity evidenced by the 2-mm shear span specimens could additionally be ascribed to the narrower shear zones obtained with the smaller shear span length, where the loading is closer to the support. The documented increase in shear strength arising out of a lower a/d ratio is in line with previous findings [26].

3.3.2 Influence of the notch depth on failure mode in quasi-static shear experiments

To investigate how the depth of the notches in shear samples affects shear failure during testing, **Fig. 14** compares the performance indices retrieved from quasi-static shear experiments for the three different notch depth values considered in this study. Varying the notch depths between 3 mm, 5 mm, and 7 mm in the quasi-static regime, as presented in experiment series 4, 2, and 6 respectively, resulted in varying the shear ligament size (*L*) for the shear sample. By decreasing notch depth, thus increasing *L*, the self-confinement of the sample increased, resulting in a remarkable amplification of the force required for leading to fracture [17]. This is shown in **Fig. 14a** and **Fig. 14c**, where the maximum force obtained was the highest for the 3-mm deep notched samples, while it decreased by 17 % for the 5-mm deep notched samples and was the least for the 7-mm deep notched samples, where a further 20 % decrease was measured. By checking the shear stress vs shear strain curves presented in **Fig. 14b** for the three notch-depth cases, the highest average shear stress was recorded for the 7-mm deep notched samples with a value of 44.5 MPa, which decreased to 35.5 MPa for the 5-mm deep notched samples. The lowest shear stress was recorded for the 3-mm deep notched samples with a value of 31 MPa, see **Fig. 14d**. Furthermore, noticeable differences in the stiffness (slopes) of the ascending branches of the shear stress vs shear strain curves were noticed. The average stiffness of the 5-mm and 7-mm deep notched samples at shear stress levels between 0 and 10 MPa were 80 MPa and 50 MPa, respectively, see **Fig. 14f**. A drastic reduction in the stiffness occurred after the shear stress level of 10 MPa up till the maximum shear stress with values of 10 MPa and 9.5 MPa, for the 5-mm and 7-mm deep notched samples, respectively, which did not highly deviate, see **Fig. 14g**. This stiffness reduction is likely due to the triggering of tensile cracks occurring at the early stage of the test, as was mentioned in Section 3.1. This phenomenon was evident in the cases of 5-mm and 7-mm deep notched samples, whereas such early tensile cracks did not form in case of 3-mm deep notched samples. The first inclined tensile crack started to form at a shear stress level between 10 MPa and 30 MPa, at which the average stiffness was 130 MPa, which is around 1.6 times higher than the initial stiffness of the 5-mm deep notched samples and 2.6 times higher than that of the 7-mm deep notched samples; see **Fig. 14f**. After a shear stress level of 30 MPa, the stiffness of the 3-mm deep notched samples reduced from 130 MPa to 30 MPa, see **Fig. 14g**. This is also demonstrated in **Fig. 14e**, where the displacement at maximum force was the lowest for the 3-mm deep notched samples. No statistically detectable difference was noted among the 5-mm and 7-mm deep notched samples.

By cross-checking the aforementioned observation with the fracture modes presented in Section 3.1, a couple of crucial design considerations on the testing configuration could be put forward. First, the highest force obtained for the 3-mm deep notched samples can be related to the elevated self-confinement undergone by those samples, which resulted in shear-compression failure, where the crushing of compression struts played the major role, as shown in **Fig. 9**. In that case, largely inclined tension cracks formed between the notches and extended outside the 2 mm shear span length, at which failure did not occur as a result of their interconnection, but rather from the crushing of the material between those cracks. With increasing notch depth from 5 mm to 7 mm, the self-confinement status decreased within the samples, resulting in a significant force reduction and a fracture mode governed by a dominant shear sliding, see **Fig. 10** and **Fig. 12**.

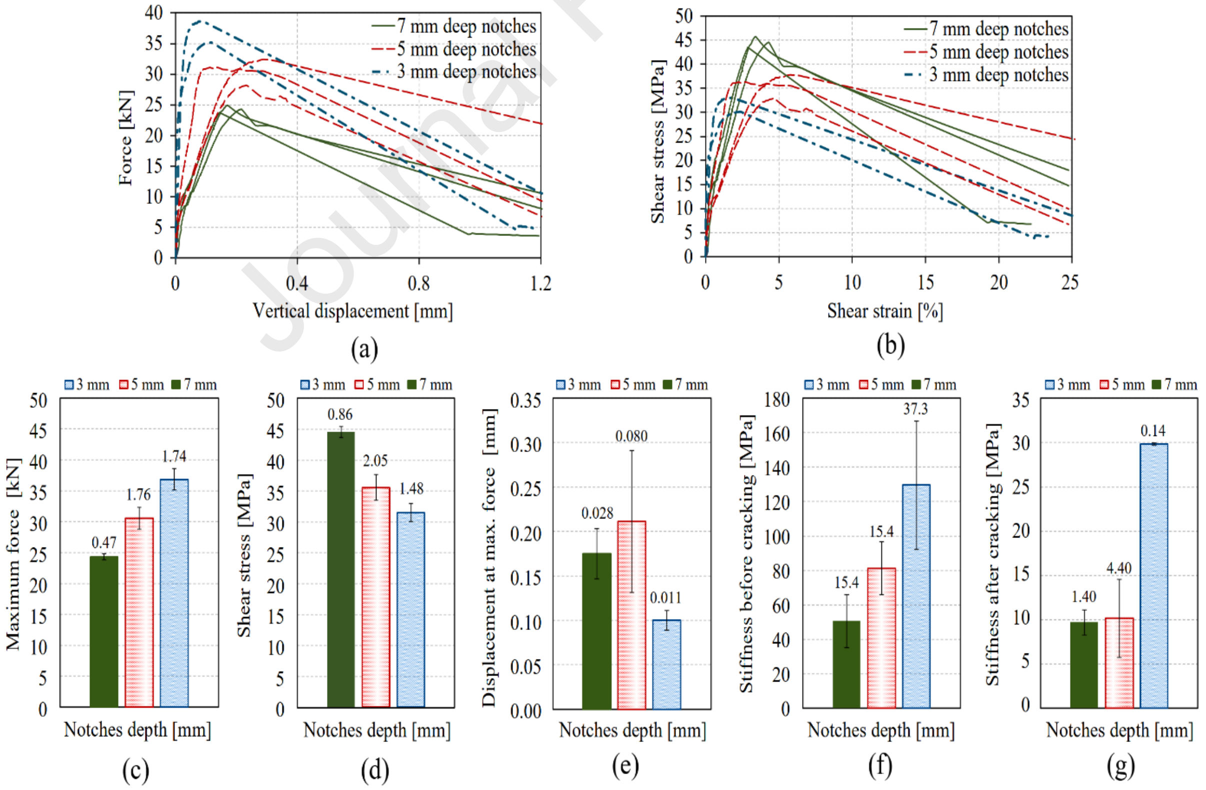

(a) (b)

(c) (d) (e) (f) (g)

Fig. 14. Quasi-static test results of shear samples with 2-mm shear span length and with notch depths of 5 mm, 3 mm, or 7 mm, experiment series 2, 4, and 6, respectively. (a) Force vs vertical displacement diagrams, (b) shear stress vs shear strain diagrams, and bar charts of (c) maximum

force, (d) shear stress, (e) displacement at maximum force, (f) stiffness before cracking, and (g) stiffness after cracking, all with respect to notches depth. Numbers above the bars represent standard deviations.

Second, the highest shear stress was recorded in the case of 7-mm deep notched samples, associated with an extremely high consistency extent, which could directly be correlated to the sharp shear sliding fracture, which was displayed by those samples, as shown in **Fig. 14b** and **Fig. 14d**. Notch depth considerably governed the location of crack initiation, the distribution of stress along the shear ligament [15], and the fracture propagation and mode of failure of the shear specimens [18,37], turning out to be a keynote parameter to be optimized when determining shear specimen shape.

Indeed, some dispersion in the results was present, which is generally aligned with normal experimental fluctuations. The coefficients of variation (CoV) for the forces and shear stresses ranged between 2 – 6 %, see **Fig. 14c** and **Fig. 14d**. Higher COVs were noticed for stiffness values, **Fig. 14f** and **Fig. 14g**, which are naturally more scattered as they are heavily affected by physical properties of the constitutive phases of SHCC (porosity, flaws, fibers, fiber/matrix bond, etc.). The highest dispersion for the displacement values was noticed for 5 mm deep notched specimens, **Fig. 14e,** which is rational due to the extent of initial tensile cracks generating in the beginning of the experiment, but are much less in the other two cases.

3.3.3 Influence of the strain rate on shear failure mode

In the impact regime, only 7-mm deep notched samples failed under the applied load (experiment series 7). A comparison between the 7-mm deep notched samples tested under quasi-static and impact regimes highlighting the influence of strain rate on SHCC response is presented in **Fig. 15**. The shear strain rate attained in the impact shear experiment of the 7-mm deep notched samples was around 2000 s^{-1}, as previously stated. The fracture modes obtained in both loading regimes were characterized by a distinct shear sliding fracture with only negligible influence of tension, as presented in **Fig. 10** and **Fig. 12**. As expected, higher force and, as a consequence, shear stress were obtained in the dynamic regime with a dynamic increase factor (DIF) at around 1.3. This DIF reflects the joint effects of strain-rate increase in addition to structural inertia, which is activated due to the accelerated mass of the shear device and the specimen. Indeed, inertia amplifies the apparent response of the shear samples, resulting in an increasing divergence from the true shear strength of the material, by increasing the strain rate [32,38,39]. The fine quantification of the force aliquot due to inertia through advanced numerical and analytical tools is necessary to determine the actual material response under impact. This issue is still being debated in the scientific community and is beyond the scope of the present contribution, currently being under further investigation.

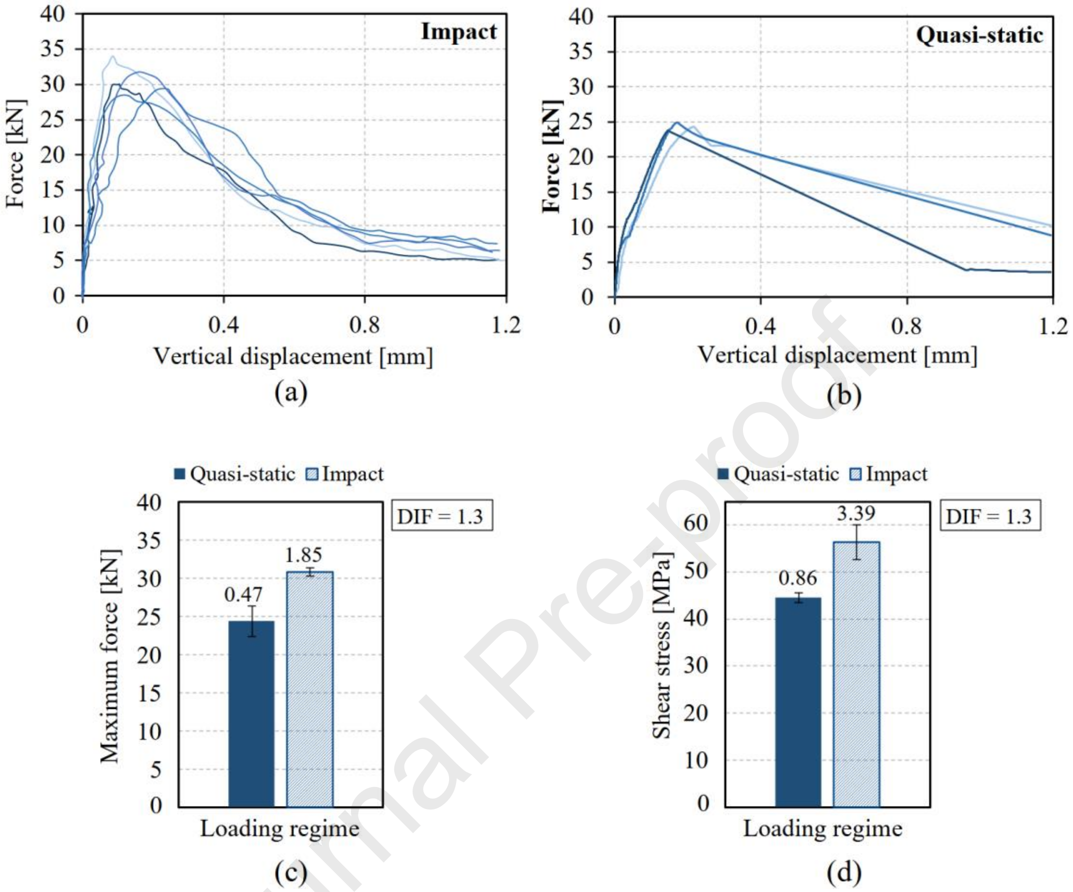

Fig. 15. Experimental results of shear samples with 2 mm shear span length and 7 mm notch depths. These force vs vertical displacement diagrams are for samples tested under (a) impact and (b) quasi-static loading regimes, experiment series 6 and 7, respectively, (c) maximum forces, and (d) shear stresses attained at each loading regime. Numbers above the bars represent standard deviations.

Shear samples with notch depths of 5 mm and 3 mm, experiment series 3 and 5 respectively, did not fail under the applied input wave. This confirms the findings obtained in the quasi-static regime, at which higher forces were attained for smaller notch depths. More specifically, in the impact regime, as even higher apparent resistance is expected, the amplitude of the applied input wave was not enough to fracture those samples, as was explained in Section 3.2. To achieve an input wave featuring higher amplitude, the setup requires an upgrade to increase the possible dropping height, resulting in higher gravitational potential energy and, accordingly, higher impact velocity and kinetic energy immediately before the collision. On the other hand, an increase in the input wave amplitude gives rise to higher strain rates that would increase the apparent response of the specimen owing to amplified structural inertia effects. That would make for incongruous comparisons with the 7-mm deep notched specimens and therefore misleading conclusions. The process of optimizing the shear device is ongoing in order to overcome the spatial restrictions imposed by the SHTB and so preventing the drop height's being increased beyond 0.65 m.

3.3.4 Limitations of the mechanical shear device

The reliability of the shear device presented in this work was successfully proven through the experimental results presented for SHCC under quasi-static and impact loads. However, some limitations pertaining the shear device still need to be addressed. First, the relatively high mass of part 1 of the device, see **Fig. 2b**, led to significant wave distortions through the input bar, so that one-dimensional wave analysis cannot be applied due to the non-equilibrium state of forces when comparing the forces measured on both bars, as explained by Tawfik et al. [23]. Second, the lateral width of the lower adapter (part 2) of the shear device (70 mm) is incompatible with the geometry of the impactor (65-mm span), which is impeded from passing through the shear device, see **Fig. 16**. This constraint significantly restricts the range of strain rates of the gravitational SHTB by limiting the dropping height of the impactor to 65 cm.

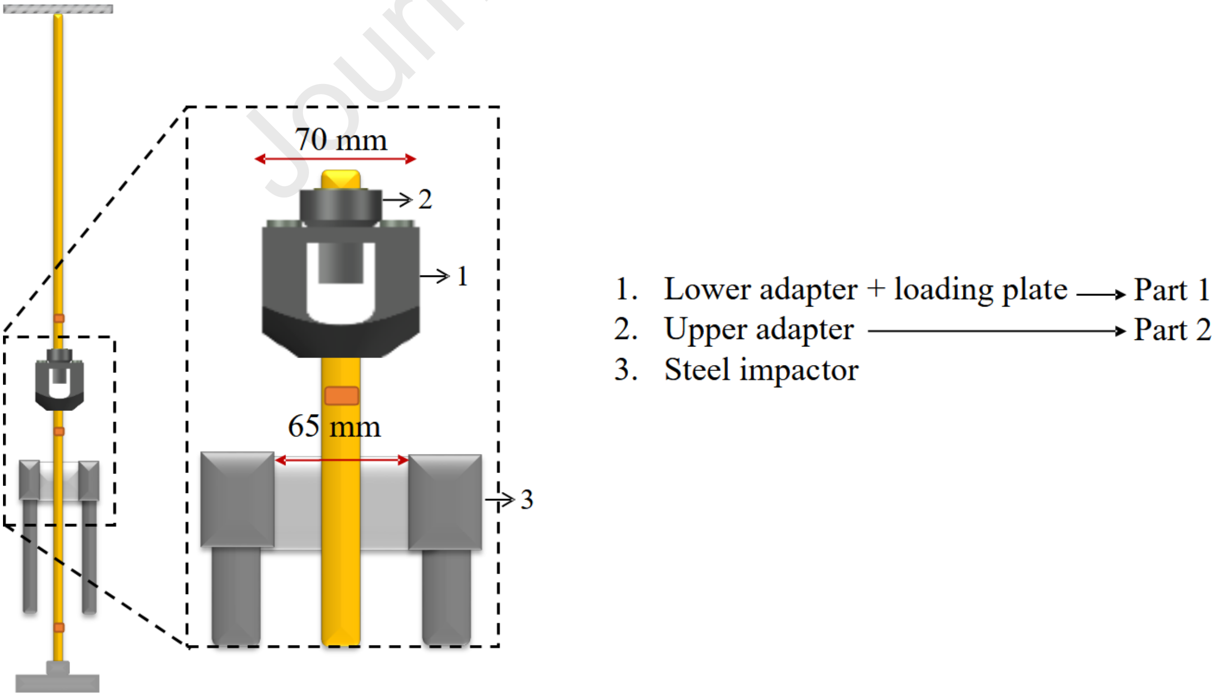

Fig. 16. SHTB illustrating the spatial restrictions, provided by the impactor, by the lower part of the shear device (part 1).

Eventually, the specimen cannot be recovered after performing the shear experiment, and therefore further microscopic analysis on the shear fracture surfaces is not possible yet. Indeed, specimens need to be extracted from the device by means of a severe heating process, which is unavoidable to remove the epoxy resin adopted to glue the specimen to the device. Such heating process compromises the fracture surfaces. It should also be mentioned that gluing the specimen provides full confinement to the sample and prevents any lateral dilation of the specimen, supporting a dominant shear failure. On the other hand, the confinement level provided by epoxy is not measured yet. Upgrading the shear device to allow for applying different levels of active confinement as well as modified geometrical features is currently under development and will be addressed in a future publication.

4 Summary and conclusions

In this work, the quasi-static and impact shear behavior of strain-hardening cement-based composites (SHCC) double-shear specimens were investigated by means of a purpose-specific, mechanical shear testing device used with a hydraulic testing machine and a newly devised gravitational Split-Hopkinson tension bar (SHTB). Digital image correlation analyses were conducted to monitor deformation and cracking pattern evolution during the experiment. The goal was to assess the most suitable set of geometrical parameters to attain a direct shear characterization of complex brittle or quasi-ductile cement-based materials. The spotlight was set on the influence of shear span length and notches depths on the shear behavior and failure mode of SHCC specimens containing ultra-high modulus polyethylene (PE) fibers. Influence of the shear span length was investigated only under the quasi-static loading regime, varying it between 5 mm and 2 mm for shear specimens with 5 mm deep notches. The influence of notch depth was investigated under both quasi-static and dynamic loading regimes, varying between 3 mm, 5 mm, and 7 mm, keeping constant the shear span length at 2 mm. The main findings obtained from this experimental work can be summarized as follows:

- Reducing the shear span length led to decreasing distance between the loading point and support, aiding localized shear zones with high shear forces as well as narrower zones for the main shear cracks to propagate. Furthermore, narrower shear zones hampered the triggering of tensile cracks therein, which weakened the materials and artificially altered the shear response being lower than expected.
- In the quasi-static loading regime, the most favorable shear failure mode was obtained in the case of 7-mm deep notched specimens, characterized by a vertical running shear

cracking causing failure to the sample after arresting of two tensile cracks initiated at the beginning of loading.

- Shallow notch depths of 3 mm caused an increase in the self-confinement of the shear sample, which resulted in the highest force required for fracture; yet the lowest shear stresses within the shear ligament. Indeed, the failure was characterized by the formation of several large tensile cracks between the top and bottom notches followed by crushing of the compression struts formed within the two shear ligaments.
- Increasing notch depth from 3 mm to 5 mm and eventually to 7 mm resulted in decreasing the force required to fracture the shear sample in combination with the highest shear stresses attained in the shear ligament, and, most remarkably, the desired dominant shear fracture.
- In the impact loading regime, the shear samples with 3-mm and 5-mm deep notches did not fracture under the given input loading wave, due to their high self-confinement. This accorded with the findings from quasi-static shear experiments, at which for the 3 mm- and 5 mm-deep notched samples, a hybrid failure mode (compression-shear) was detected at higher force levels.
- The shear samples with 7-mm-deep notches tested in impact regime showed an obvious shear fracture with a dominant crack sliding (Mode II), aligned with the consistency of the behavior and fracture mode obtained from quasi-static experiments. This specific specimen configuration is therefore the most suitable for an accurate direct quantification of the shear properties of complex quasi-ductile mineral-based materials, within an optimized gravity-based SHTB testing setup.

Although the considerations on the optimized parameters were based on testing one material combination only, i.e., SHCC with 2% PE fibers, their validity can be extended for different fiber dosages, length or diameter. Indeed, the investigated parameters mainly pertain to the loading configuration, by promoting dominant shear fracture mode, associated with significant reduction of undesired tensile and bending effects. Preserving the nature of the failure mode by selecting proper geometrical features of shear samples enables the sound characterization of a wide range of composite systems, which is the focus of an upcoming publication. Furthermore, the 2 mm shear span length was selected as an optimum length and not further reduced due to few reasons. First, the shear fracture mode required was already achieved with the 2 mm shear span length in combination with the 7 mm deep notches. Second, further reduction of the shear span length may result in high localized compressive stresses just at the notches edges, which might cause local crushing at the notches areas. Third, the over-reduced shear span length would introduce more difficulties in impact testing, as stronger illumination would be required due to the very low exposure times, to optically monitor the specimen's surface, which is a challenging task.

CRediT authorship contribution statement

Ahmed Tawfik: Conceptualization, Methodology, Software, Validation, Formal analysis, Investigation, Data curation, Visualization, Writing – original draft, Writing – review & editing. **Cesare Signorini:** Conceptualization, Supervision, Investigation, Writing – review & editing. **Viktor Mechtcherine:** Funding acquisition, Project administration, Resources, Supervision, Writing – review & editing.

Acknowledgements

The financial support of the German Research Foundation (*Deutsche Forschungsgemeinschaft*, DFG) within the Research Training Group GRK 2250/2 "Mineral-bonded composites for enhanced structural impact safety", project number 287321140, is gratefully acknowledged. The authors express their gratitude to Kai Uwe Mehlisch and Tilo Günzel for their contribution in setting up the testing facilities.

References

[1] V. Li, On engineered cementitious composites (ECC). A review of the material and its applications, J. Adv. Concr. Technol. 1 (2003) 215–230. http://jlc.jst.go.jp/JST.JSTAGE/jact/1.215?from=Google.

[2] V.C. Li, S. Wang, C. Wu, Tensile strain-hardening behavior of polyvinyl alchohol engineered cementitious composite (PVA-ECC), (2001).

[3] M. Maalej, S.T. Quek, S.F.U. Ahmed, J. Zhang, V.W.J. Lin, K.S. Leong, Review of potential structural applications of hybrid fiber Engineered Cementitious Composites, Constr. Build. Mater. 36 (2012) 216–227. https://doi.org/10.1016/j.conbuildmat.2012.04.010.

[4] S. Pourfalah, D.M. Cotsovos, B. Suryanto, M. Moatamedi, Out-of-plane behaviour of masonry specimens strengthened with ECC under impact loading, Eng. Struct. 173 (2018) 1002–1018. https://doi.org/10.1016/j.engstruct.2018.06.078.

[5] V.C. Li, From micromechanics to structural engineering -the design of cementitious composites for civil engineering applications, Struct. Eng. Eng. 10 (1994) 1–34.

[6] I. Curosu, V. Mechtcherine, D. Forni, E. Cadoni, Performance of various strain-hardening cement-based composites (SHCC) subject to uniaxial impact tensile loading, Cem. Concr. Res. 102 (2017) 16–28. https://doi.org/10.1016/j.cemconres.2017.08.008.

[7] I. Curosu, M. Liebscher, V. Mechtcherine, C. Bellmann, S. Michel, Tensile behavior of high-strength strain-hardening cement-based composites (HS-SHCC) made with high-

performance polyethylene, aramid and PBO fibers, Cem. Concr. Res. 98 (2017) 71–81. https://doi.org/10.1016/j.cemconres.2017.04.004.

[8] A.A. Heravi, I. Curosu, V. Mechtcherine, A gravity-driven split Hopkinson tension bar for investigating quasi-ductile and strain-hardening cement-based composites under tensile impact loading, Cem. Concr. Compos. 105 (2020) 103430. https://doi.org/10.1016/j.cemconcomp.2019.103430.

[9] A.A. Heravi, O. Mosig, V. Mechtcherine, A. Tawfik, M. Curbach, An experimental investigation of the behavior of strain-hardening cement-based composites (Shcc) under impact compression and shear loading, Materials (Basel). 13 (2020) 1–19. https://doi.org/10.3390/ma13204514.

[10] T. Kanda, Application of Pseudo Strain Hardening Cementitious Composites To Shear Resistant Structural ..., (2016).

[11] Y. Zhang, W. Lv, H. Peng, Shear Resistance Evaluation of Strain-Hardening Cementitious Composites Member, Int. J. Civ. Eng. 16 (2018) 255–261. https://doi.org/10.1007/s40999-016-0123-1.

[12] Y.X. Zhang, N. Ueda, Y. Umeda, H. Nakamura, M. Kunieda, Evaluation of shear failure of Strain Hardening Cementitious Composite beams, Procedia Eng. 14 (2011) 2048–2057. https://doi.org/10.1016/j.proeng.2011.07.257.

[13] V.C. Li, D.K. Mishra, A.E. Naaman, J.K. Wight, J.M. LaFave, H.C. Wu, Y. Inada, On the shear behavior of engineered cementitious composites, Adv. Cem. Based Mater. 1 (1994) 142–149. https://doi.org/10.1016/1065-7355(94)90045-0.

[14] T. Kanakubo, K. Shimizu, S. Nagai, T. Kanda, Shear transmission on crack surface of ECC, Proc. Fram. Jeju. 13 (2010) 1623–1630.

[15] Q. Shang, G.P.A.G. Van zijl, Characterising the shear behaviour of strain- hardening fi bre-reinforced cement-based composites, 49 (2007) 16–23.

[16] T.C.S.P. Figueiredo, I. Curosu, G.L.G. Gonzáles, M. Hering, F. de A. Silva, M. Curbach, V. Mechtcherine, Mechanical behavior of strain-hardening cement-based composites (SHCC) subjected to torsional loading and to combined torsional and axial loading, Mater. Des. 198 (2021). https://doi.org/10.1016/j.matdes.2020.109371.

[17] B. Lukić, P. Forquin, Experimental characterization of the punch through shear strength of an ultra-high performance concrete, Int. J. Impact Eng. 91 (2016) 34–45.

[18] E. Cadoni, M. Dotta, D. Forni, G. Riganti, Dynamic response of UHPFRCs in direct-shear tests, Procedia Struct. Integr. 28 (2020) 933–942. https://doi.org/10.1016/j.prostr.2020.11.066.

[19] J.D. Campbell, W.G. Ferguson, The temperature and strain-rate dependence of the shear strength of mild steel, Philos. Mag. 21 (1970) 63–82. https://doi.org/10.1080/14786437008238397.

[20] W.G. Ferguson, F.E. Hauser, J.E. Dorn, Dislocation damping in zinc single crystals, J Appl. Phys., 49 (1966) 15–19. https://doi.org/10.1111/j.1151-2916.1966.tb13138.x.

[21] Y. Guo, Y. Li, A novel approach to testing the dynamic shear response of Ti-6Al-4V, Acta Mech. Solida Sin. 25 (2012) 299–311. https://doi.org/10.1016/S0894-9166(12)60027-5.

[22] Z. Xu, X. Ding, W. Zhang, F. Huang, A novel method in dynamic shear testing of bulk

materials using the traditional SHPB technique, Int. J. Impact Eng. 101 (2017) 90–104. https://doi.org/10.1016/j.ijimpeng.2016.11.012.

[23] A. Tawfik, I. Curosu, G. Alsous, V. Mechtcherine, A testing setup for investigating quasi-ductile and strain-hardening, cement-based composites (SHCC) under impact shear loading, Int. J. Impact Eng. (2022).

[24] J. Magnusson, M. Hallgren, A. Ansell, Shear in concrete structures subjected to dynamic loads, Struct. Concr. 15 (2014) 55–65.

[25] B. Barr, M. Derradj, Numerical study of compact shear (Mode II) type test specimen geometry, Mater. Struct. Constr. 41 (2008) 1203–1210. https://doi.org/10.1617/s11527-007-9318-x.

[26] T. Thuong, J. Kil, S. Pyo, D. Joo, Shear resistance of ultra-high-performance fiber-reinforced concrete, Constr. Build. Mater. 151 (2017) 246–257.

[27] DSM Dyneema, Ultra High Molecular Weight Polyethylene Fiber from DSM Dyneema, Tech. DataSheet. 49 (2016) 1–4. https://issuu.com/eurofibers/docs/name8f0d44.

[28] A. Tawfik, I. Curosu, V. Mechtcherine, Mechanical characterization of strain-hardening cement based composites (SHCC) under impact shear load, EPJ Web Conf. 250 (2021) 01021. https://doi.org/10.1051/epjconf/202125001021.

[29] A. Chatterjee, A.L. Ruina, Two Interpretations of Rigidity in Rigid Body Collisions, ASME Int. Mech. Eng. Congr. Expo. Proc. 1997-AC (1997) 47–55. https://doi.org/10.1115/IMECE1997-0522.

[30] A. Heravi, V. Mechtcherine, Mechanical characterization of strain-hardening cement-based composite (SHCC) under dynamic tensile load, in: Fram. 10th Int. Conf., 2019.

[31] F.E. Hauser, Techniques for measuring stress-strain relations at high strain rates, Exp. Mech. 6 (1966) 395–402. https://doi.org/10.1007/bf02326284.

[32] J. Ožbolt, A. Sharma, B. Irhan, E. Sola, Tensile behavior of concrete under high loading rates, Int. J. Impact Eng. 69 (2014) 55–68.

[33] T.T. NGO, D.J. KIM, Shear stress versus strain responses of ultra-high-performance fiber-reinforced concretes at high strain rates, Int. J. Impact Eng. 111 (2018) 187–198. http://dx.doi.org/10.1016/j.ijimpeng.2017.09.010.

[34] GOM, Digital image correlation and strain computation basics, GOM Test. Tech. Doc. V8 SR1 (2016) 1–30.

[35] Z.P. Bažant, P.A. Pfeiffer, Shear fracture tests of concrete, Mater. Struct. 19 (1986) 111–121. https://doi.org/10.1007/BF02481755.

[36] P.A. Pfeiffer, A.H. Marchertas, Z.P. Bazant, Blunt Crack Bank Propagation in Finite Element Analysis for Concrete Structures., Trans. Int. Conf. Struct. Mech. React. Technol. (1983).

[37] T. Backers, O. Stephansson, ISRM suggested method for the determination of mode II fracture toughness, Rock Mech. Rock Eng. 45 (2012) 1011–1022. https://doi.org/10.1007/s00603-012-0271-9.

[38] E.A. Flores-Johnson, Q.M. Li, Structural effects on compressive strength enhancement of concrete-like materials in a split Hopkinson pressure bar test, Int. J. Impact Eng. 109 (2017) 408–418.

[39] S. Zhang, Y. Lu, X. Jiang, W. Jiang, Inertial effect on concrete-like materials under

dynamic direct tension, Int. J. Prot. Struct. 9 (2018) 377–396. https://doi.org/10.1177/2041419618766156.

Declaration of interests

☒ The authors declare that they have no known competing financial interests or personal relationships that could have appeared to influence the work reported in this paper.

☐ The authors declare the following financial interests/personal relationships which may be considered as potential competing interests: